DOI: 10.1002/ejic.200700049

Reactions of 1,2,4-Trithiolane, 1,2,5-Trithiepane, 1,2,5-Trithiocane and 1,2,6-Trithionane with Nonacarbonyldiiron: Structural Determination and Electrochemical Investigation

Jochen Windhager,[a] Manfred Rudolph,*[a] Silvio Bräutigam,[a] Helmar Görls,[a] and Wolfgang Weigand*[a]

Dedicated to Prof. Wolfgang Beck on the occasion of his 75th birthday

Keywords: Iron / Cluster compounds / S ligands / Hydrogenase / Electrocatalysis / Dihydrogen

The reactions of 1,2,4-trithiolane (**1**), 1,2,5-trithiepane (**6**), 1,2,5-trithiocane (**12**) and 1,2,6-trithionane (**10**) with nonacarbonyldiiron (**2**) have been investigated. A novel diiron model complex, which can serve as a model complex of the active site of [Fe-only]-hydrogenase, was formed from the reaction with **1**. In contrast, the reaction of **6** with **2** afforded the trinuclear iron cluster **7**. Interestingly, the diiron compound **11** was obtained with 1,2,6-trithionane (**10**), which can be attributed to the more flexible dithiolato ligand **10**. Furthermore, the reaction with 1,2,5-trithiocane (**12**) yielded the trinuclear cluster **13**. X-ray structure analyses were performed on compounds **3**, **7**, **10**, **11** and **13**. The reactions of the reduced iron species **3** with pivalic acid (HP) were studied electrochemically. The most significant features of the experimental cyclic voltammograms (CVs) could be reproduced by digital simulation on the basis of a reaction scheme that includes both the coordination of HP as well as the catalytic generation of hydrogen.

Introduction

The recent generation of thiosulfine **A** and the first dithiirane **B** by flash vacuum pyrolysis (FVP) of 1,2,4-trithiolane (**1**), in argon matrices at 10 K, was monitored by both IR and UV/Vis spectroscopy (Scheme 1).[1] In 1993, Nakayama and Ishii et al. reported the first synthesis of stable dithiirane.[2] We have shown that platinum(0) complexes, for instance $Pt(\eta^2\text{-}C_2H_4)(Ph_3P)_2$, react with 1,2,4-trithiolane (**1**) by insertion along the S–S bond. When two equivalents of the platinum(0) complex were used, dithiolatoplatinum(II) **C** was obtained (Scheme 2). This complex decomposed to give the –platinum complex **E** and the methylenedithiolato complex **D**.[3]

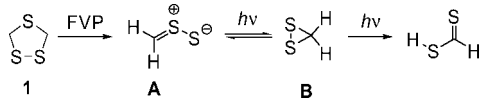

Scheme 1. Flash vacuum pyrolysis (FVP) of 1,2,4-trithiolane **1**.

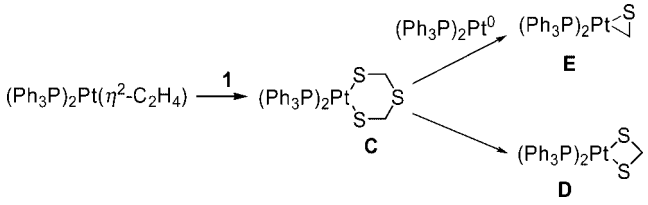

Scheme 2. Treatment of 2 equiv. $Pt(\eta^2\text{-}C_2H_4)(Ph_3P)_2$ with 1,2,4-trithiolane (**1**) to give a 1:1 mixture of methylenedithiolato complex **D** and thioformaldehyde complex **E**.

The oxidative addition of low-valent metal complexes to cyclic disulfides has received significant attention in recent years.[4] As an extension of previous work, reaction of **1** with nonacarbonyldiiron (**2**) was conducted to investigate whether **2** would insert into the S–S bond with the formation of a novel type of dithiolato-bridged diiron complex, which can serve as a model for the active site of [Fe-only]-hydrogenases. Since the first X-ray structure determination of [Fe-only]-hydrogenase was reported,[5] several research groups have prepared simple dinuclear iron complexes that have structural, spectroscopic and functional properties similar to those of the active site of [Fe-only]-hydrogenase.[6] Moreover, the two iron atoms in the active site are bridged by a three-atom-linked dithiolato ligand SCH_2XCH_2S;

[a] Institut für Anorganische und Analytische Chemie, Friedrich-Schiller Universität Jena,
August-Bebel-Strasse 2, 07743 Jena, Germany
Fax: +49-3641-948102
E-mail: c8wewo@uni-jena.de
Supporting information for this article is available on the WWW under http://www.eurjic.org or from the author.

however, the nature of the X group remains unclear. Nevertheless, it has been postulated that X is an NH unit that is hydrogen bonded to a nearby cysteine-SH unit.[5a]

In order to elucidate the influence of the X group on the hydrogenase activity, we set out to prepare model complexes with X = S by reaction of **1** with **2**. We also tested the reactivity of 1,2,5-trithiepane (**6**), 1,2,5-trithiocane (**13**) and 1,2,6-trithionane (**10**) towards **2** to determine the role of the length of the dithiolate linker in the model complexes (Scheme 3). Very recently, Darensbourg and Hall et al. performed theoretical calculations to determine the influence of the nature of X and the lengthening of the dithiolato bridge on the conformational structure of the model complexes.[7]

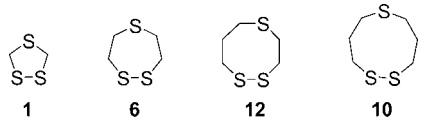

Scheme 3. The sulfur heterocycles **1**, **6**, **10** and **12**.

Results and Discussion

Reaction of $Fe_2(CO)_9$ (2) with 1,2,4-Trithiolane (1)

Treatment of 3 equiv. $Fe_2(CO)_9$ (**2**) with 1 equiv. 1,2,4-trithiolane (**1**) in thf for 15 min at 65 °C afforded a mixture of three compounds **3**–**5**, which were separated and isolated by using column chromatography (Scheme 4).

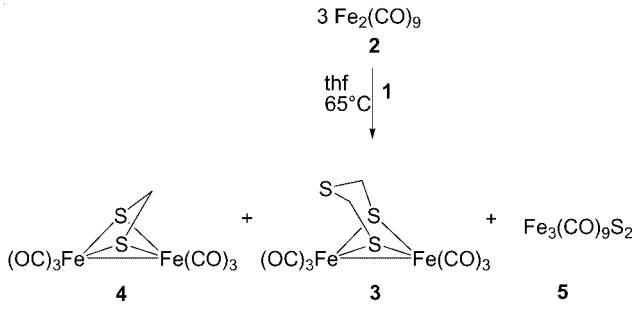

Scheme 4. Reaction of 3 equiv. $Fe_2(CO)_9$ (**2**) with 1 equiv. 1,2,4-trithiolane (**1**).

The ^{1}H NMR spectra of **3** and **4** shows one singlet each at δ = 3.21 and 4.61 ppm, respectively. On the basis of the ^{1}H and ^{13}C NMR spectroscopic data, compound **4** was identified as the known methylenedithiolato-bridged compound.[8] The crystal data of product **5** confirms the presence of a trinuclear complex $Fe_3S_2(CO)_9$.[9] MS analysis shows the stepwise fragmentation of six CO groups and the molecular peak at *m*/*z* = 404 for product **3**, which suggests the presence of a diiron hexacarbonyl complex fragment coordinated to the sulfurdithiolato ligand (SDT). Single-crystal X-ray analysis reveals the proposed structure of **3** (Figure 1); the iron coordination geometry in **3** is rather similar to that in its oxadithiolate (ODT) analogue $Fe_2(\mu\text{-}SCH_2OCH_2S\text{-}\mu)(CO)_6$.[6i] The Fe–Fe bond length in **3** is 2.5120(5) Å, a value very similar to those in the propanedithiolate (PDT) analogue [2.5103(11) Å][6a–6d] and in the ODT analogue [2.5113(13) Å],[6i,6l] but slightly longer (0.02 Å) than that in the azadithiolato (ADT) complex [2.4924(7) Å].[6e–6g] The Fe–Fe bond in **3** is slightly shorter than those reported for the oxidised state diiron subsite (2.62 and 2.60 Å) and that in the reduced state diiron subsite of the enzyme structure (2.55 Å).[5a] Similar to the ODT complex, the bridgehead sulfur atom is disordered (50%).

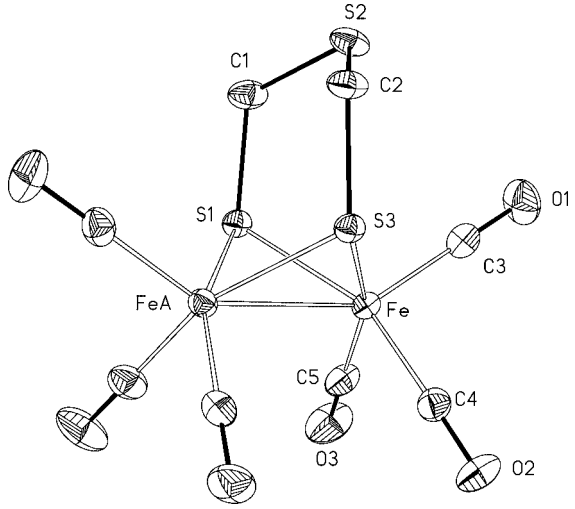

Figure 1. Structure of $Fe_2(SDT)(CO)_6$ (**3**) with thermal ellipsoids set at the 50% probability level (hydrogen atoms are omitted for clarity). Selected distances [Å] and angles [°]: Fe–FeA 2.5120(5), Fe–C3 1.800(9), Fe–C4 1.794(5), Fe–C5 1.800(8), Fe–S1 2.2514(5), Fe–S3 2.2557(7); Fe–S1–FeA 67.672(19), Fe–S3–FeA 67.82(2).

Reaction of $Fe_2(CO)_9$ (2) with 1,2,5-Trithiepane (6)

By analogy with 1,2,4-trithiolane (**1**), the reaction of 1,2,5-trithiepane (**6**) with **2** was carried out in thf for 15 min at 65 °C. The crude mixture was separated by using column chromatography. Products **7** and **8** were isolated as analytically pure orange and green solids, respectively. For compound **8**, the ^{1}H NMR analysis reveals one singlet at δ = 2.34 ppm. Oxidation of **8** with excess dimethyldioxirane (DMD) quantitatively afforded complex **9**, which was subsequently analysed by X-ray diffraction analysis (Scheme 5). Compounds **8** and **9** have been mentioned previously in the literature.[10]

^{1}H-^{1}H COSY and ^{1}H-^{13}C HSQC spectra of **7** reveal four groups of ^{1}H resonances in a 1:1:1:1 ratio as well as two ^{13}C signals at δ = 39.68 and 45.59 ppm. DEI-MS shows the $[M]^+$ ion at *m*/*z* = 572, with the stepwise fragmentation of nine CO groups. On the basis of spectroscopic data, it is suggested that **7** consists of more than two $Fe(CO)_3$ moieties, a result that is further confirmed by the X-ray structure analysis as a trinuclear cluster. The isostructural ruthenium cluster was synthesised by the reaction of $Ru_3(CO)_{12}$ and 1,4,7-trithiacyclononane (9S3) in thf.[11] Alternatively, when the complex $Ru_3(CO)_7(\mu\text{-}CO)_2(1,1,1\text{-}\eta^3\text{-}9S3)$ is heated at reflux for 16 h, an analogous ruthenium cluster is obtained.[12]

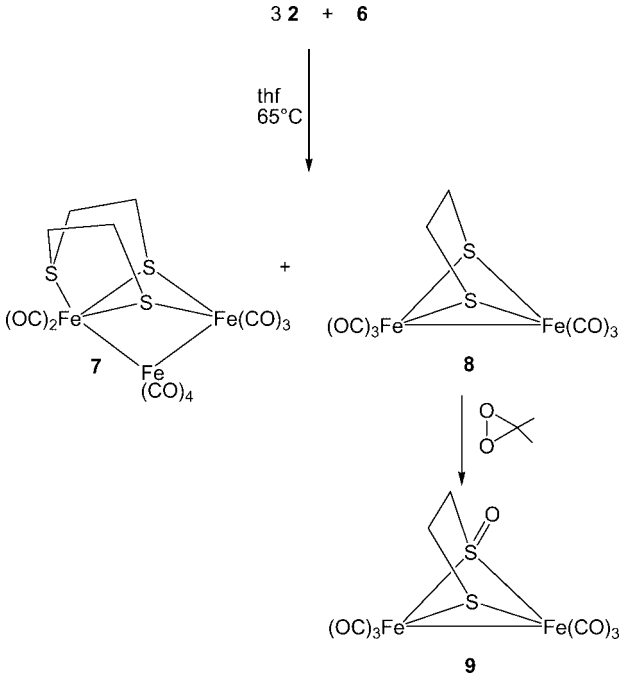

Scheme 5. Reaction of 1,2,5-trithiepane (**6**) with **2**.

As shown in Figure 2, all iron atoms display a distorted octahedral coordination geometry. The Fe1 and Fe2 centres are μ^2-bridged by the bis(thiolatoethylene sulfide) ligand (BTES). Because of the two additional methylene groups in the BTES ligand relative to that in **3**, the thioether S atom coordinates to Fe1. A similar motif was also observed in the complex $[(ON)Ni(\mu\text{-BTES})Fe(NO)_2]$.[13]

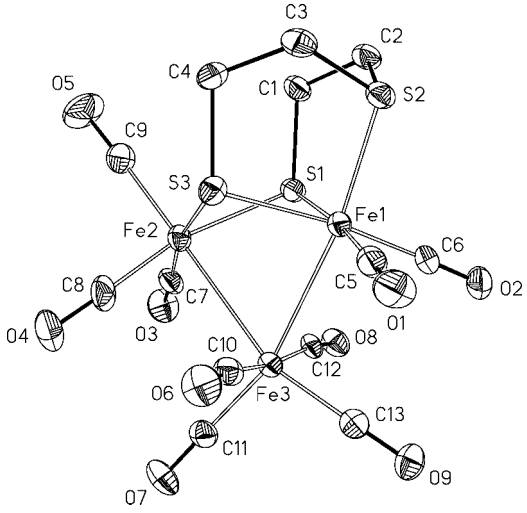

Figure 2. Structure of $Fe_3(\mu\text{-BTES})(CO)_9$ (**7**) with thermal ellipsoids set at the 50% probability level (hydrogen atoms are omitted for clarity). Selected distances [Å] and angles [°]: Fe1–Fe3 2.7355(13), Fe2–Fe3 2.7622(14), Fe1–S1 2.314(2), Fe1–S3 2.302(2), Fe2–S1 2.317(2), Fe2–S3 2.318(2), Fe2–S2 2.250(2); Fe1–S1–Fe2 81.92(6), Fe1–S3–Fe2 82.18(7).

The Fe–S bond lengths for the bridging sulfur atoms in **7** are 2.312 Å (mean), but the Fe1–S2 bond is remarkably shorter [2.250(2) Å]. The Fe1–S1/S3–Fe2 angles of 81.92(6)° and 82.18(7)° differ significantly from the corresponding angles in **3**, 67.82(2)° and 67.67(2)°, respectively. Accordingly, the Fe1···Fe2 distance in **7** (3.036 Å) is significantly longer than that in **3** [2.5120(5) Å]. As a consequence, a $Fe(CO)_4$ fragment inserts into the Fe1 and Fe2 bond, leading to cluster species **7**, a cluster with a total electron count of 50, which is classified as hypho according to the Wade–Mingos rules.

Reactions of $Fe_2(CO)_9$ (2) with 1,2,6-Trithionane (10)

1,2,6-Trithionane (**10**) was conveniently obtained by a reported procedure.[14] Colourless needles that were suitable for X-ray diffraction analysis were obtained by recrystallising **10** from hexane at –25 °C. The nine-membered ring shows a nonplanar structure (Figure 3) with a for C3–S3–S4–C4 torsion angle of 60.62(15)°. The S3–S4 bond is 1.993(3) Å and is slightly shorter than the corresponding bond in $\alpha\text{-}S_8$ (2.05 Å).[15]

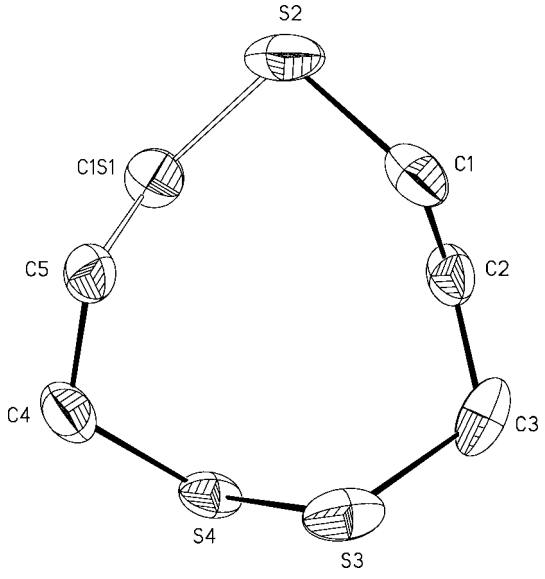

Figure 3. Structure of 1,2,6-trithionane (**10**) with thermal ellipsoids set at the 50% probability level (hydrogen atoms are omitted for clarity). Selected distances [Å] and angles [°]: S3–S4 1.993(3); C3–S3–S4–C4 60.62(15)°.

When **10** was treated with 3 equiv. **2** in thf at 65 °C, a red-brown solution was obtained. After 15 min, the reaction was complete, and compound **11** was isolated after workup as a brown solid by column chromatography (Scheme 6).

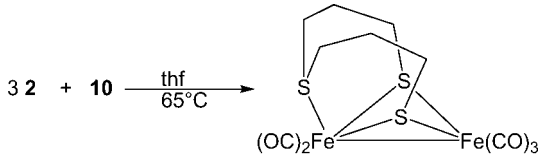

Scheme 6. Reaction of 1,2,6-trithionane (**10**) with **2**.

^1H-^1H COSY and ^1H-^{13}C HSQC analysis of **11** allowed the assignment of the ^{13}C resonances at δ = 18.90 and 27.01 ppm to the C5 and C2 atoms, respectively; the reso-

nances at 28.41 and 28.47 ppm are assigned to the C1 and C6 atoms and those at 36.72 and 37.56 ppm to the C3 and C4 atoms, respectively. The latter 4 carbon atoms are directly connected to the thiolato groups and thioether group, respectively. All signals in the ^{1}H NMR spectrum are assigned to the 12 diastereotopic protons. DEI-MS reveals the $[M]^+$ ion at m/z = 432 and a stepwise fragmentation of five CO groups. These results indicate the formation of a diiron complex with both $Fe(CO)_2$ and $Fe(CO)_3$ moieties.

This structural motif was confirmed by X-ray diffraction (Figure 4). Red-brown crystals of **11** were obtained from hexane at –25 °C. The crystals were stable in air for weeks at room temperature, but decomposed in solution under argon above 0 °C within one day to form an insoluble brown solid. Complex **11** displays two five-coordinate iron centres with square-pyramidal geometry and an Fe–Fe bond length of 2.5016(5) Å, which is slightly shorter than that in **3**. Complex **11** may be compared with $[Fe_2\{MeSCH_2C(Me)(CH_2S)_2\}(CO)_5]$, showing a similar Fe–Fe distance [2.5086(9) Å].[16]

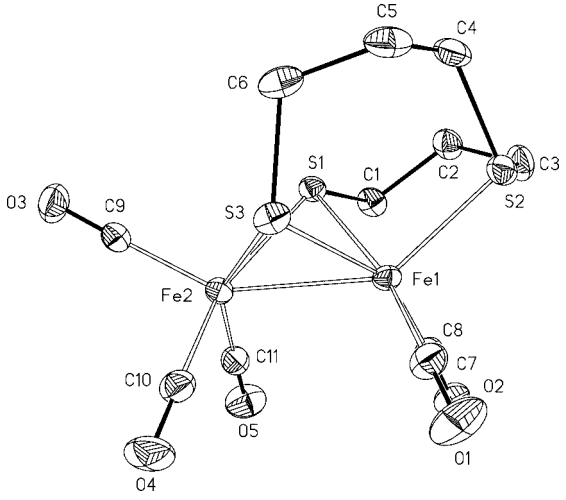

Figure 4. Structure of $Fe_2(\mu$-BTPS$)(CO)_5$ (**11**) with thermal ellipsoids set at the 50% probability level (hydrogen atoms are omitted for clarity). Selected distances [Å] and angles [°]: Fe1–Fe2 2.5016(5), Fe1–S1 2.2568(7), Fe1–S3 2.2448(8), Fe2–S1 2.2481(7), Fe2–S3 2.3040(8), Fe1–S2 2.2449(7); Fe1–S1–Fe2 67.46(2), Fe1–S3–Fe2 66.71(2).

The thiolato sulfur atoms S1 and S3 are μ^2-coordinated to Fe1 and Fe2. In addition, the thioether atom (S2) is connected to Fe1. The angles Fe1–S1–Fe2 [67.46(2)°] and Fe1–S3–Fe2 [66.71(2)°] compare well to those in **3** [67.82(2)° and 67.67(2)°], but in contrast to **3**, **11** does not contain a mirror plane. The presence of the extra methylene groups in **11** relative to **7** reduces steric strain and thus provides the BTPS ligand with more flexibility, which enables the coordination of the thioether S2 atom to Fe1 with the formation of a Fe–Fe bond. With the exception of the Fe2–S3 bond length [2.3040(8) Å], the remaining Fe–S distances are quite similar [2.2448(8), 2.2449(7), 2.2481(7), 2.2568(7) Å].

Reactions of $Fe_2(CO)_9$ (2) with 1,2,5-Trithiocane (12)

In order to elucidate the influence of the size of the dithiolato thioethers on the structure of the iron complexes, we also treated **12** with **2** at 65 °C in thf. After workup, compounds **8** and **13** were isolated by column chromatography (Scheme 7). Additionally, two green side-fractions were obtained, but unfortunately, we have not been able to characterise them yet. The fraction containing **13** was dissolved in chloroform. After diffusion of pentane into the concentrated solution, red-brown crystals were afforded after 2 d at 0 °C.

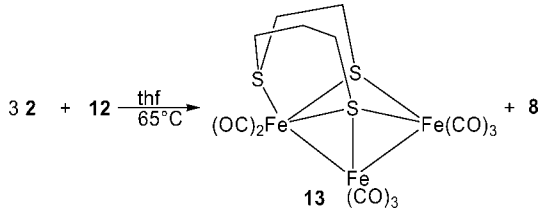

Scheme 7. Reaction of 1,2,5-trithiocane (**12**) with **2**.

The ^{1}H-^{1}H COSY spectrum of **13** shows ten groups of resonance signals, which were assigned to the ten diastereotopic protons. According to the ^{1}H-^{1}H COSY and ^{1}H-^{13}C HSQC spectra of **13**, the ^{13}C resonances at δ = 34.54 and 34.75 ppm are attributed to the carbon atoms of the ethylene group [C1 and C2] and the signals at 25.41, 31.71 and 36.92 ppm to the C4, C5 and C3 atoms, respectively. DEI-MS reveals the $[M]^+$ ion at m/z = 558 and a stepwise fragmentation of eight CO groups.

As shown in Figure 5, complex **13** has a distorted "non-closed" square-pyramidal Fe_3S_2 core with Fe1–Fe2, Fe2–Fe3 and Fe2–S3 distances of 2.7352(9), 2.6888(9) and 2.1173(12) Å, respectively. As in the molecular structure of **7**, all iron atoms have a distorted octahedral coordination geometry. The geometry of Fe1–S1–Fe3–S3 is almost square planar, with a mean deviation from planarity of 0.0941 Å. The Fe1–S1–Fe3 angle of 93.65(4)° and Fe1–S3–Fe3 angle of 100.56(4)° are significantly larger than the corresponding angles in **7** [81.92(6)° and 82.18(7)°]. As a result, the Fe1···Fe3 distance is considerably longer (3.376 Å) than the corresponding distance in **7**. The 3-(2-thiolatoethylthio)-propane-1-thiolato ligand is coordinated to the Fe1 and Fe3 atoms, but the S3 atom is μ^3-coordinated to the three iron atoms as a result of the almost planar geometry of the Fe1–S1–Fe3–S3 moiety, which is remarkably different from that observed in **7**. Therefore, instead of an $Fe(CO)_4$ unit as in **7**, an $Fe(CO)_3$ complex fragment coordinates in **13**, which leads to an arachno cluster. In contrast to compound **7**, the Fe–S distances are quite different from each other. The Fe1–S1 [2.3255(12) Å] and Fe3–S1 [2.3042(12) Å] bonds are significantly longer than the Fe1–S3 [2.2040(12) Å] and Fe3–S3 [2.1854(12) Å] bonds, which can be attributed to the larger strain caused by the ethylenethiolato group than that caused by the propylenethiolato group.

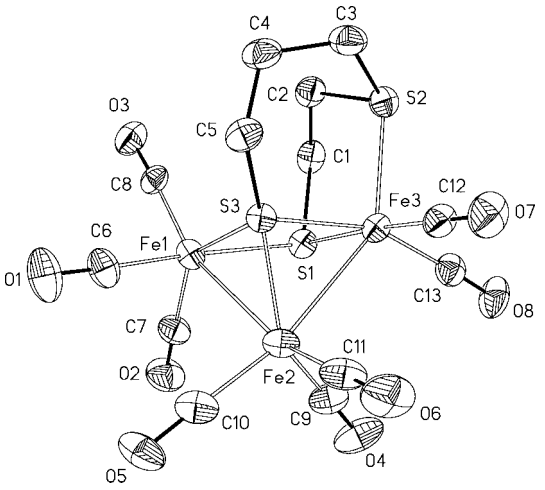

Figure 5. Structure of $Fe_3(S(CH_2)_2S(CH_2)_3S)(CO)_8$ (**13**) with thermal ellipsoids set at the 50% probability level (hydrogen atoms are omitted for clarity). Selected distances [Å] and angles [°]: Fe1–Fe2 2.7352(9), Fe2–Fe3 2.6888(9), Fe1–S1 2.3255(12), Fe1–S3 2.2040(12), Fe3–S1 2.3042(12), Fe3–S3 2.1854(12), Fe2–S3 2.1173(12), Fe3–S2 2.2545(13); Fe1–S1–Fe3 93.65(4), Fe1–S3–Fe3 100.56(4).

Electrochemical Investigations

The electrochemical behaviour of **3** was studied in the aprotic solvent acetonitrile by varying the concentration of pivalic acid (denoted as HP). This Brønsted acid is electrochemically inactive in the required potential range so that site effects originating from the steady-state concentration of electrochemically produced radicals can be excluded. Moreover, the use of pivalic acid in anhydrous acetonitrile leads to the favourable situation in which catalytic hydrogen generation does not occur in the potential range where the two-electron reduction of the iron species proceeds. Unlike the processes reported, for instance, by Best, Pickett et al.[17] or those for the system denoted as **1-P** by Darensbourg et al.[18c] and Rauchfuss et al.[18a,18b] in which the overall current is dominated by the catalytic reactions as soon as acid is present, the interaction between reduced iron species and pivalic acid that occurs prior to the catalytic cycle can be studied independently in a well-separated potential range. A similar situation was observed for the model system 1 of the above-mentioned articles by Darensbourg and Rauchfuss et al.[18]

Electrochemistry of 3 in the Absence of Pivalic Acid

The solid lines in Figure 6 show the cyclic voltammetric reduction of **3** in acetonitrile measured by varying the scan rate from 5 to 200 V s^{-1}. The open-circle traces show theoretical CVs simulated on the basis of the following reaction scheme (**3** is denoted as Fe–Fe).

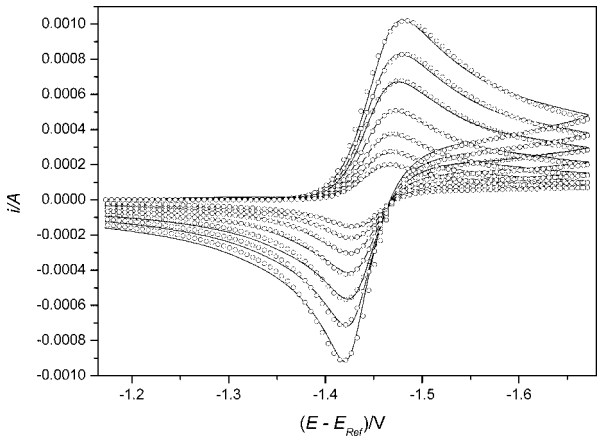

Figure 6. Experimental (solid lines) and simulated (open circles) CVs for the reduction of 2.46 mM **3** in acetonitrile with scan rates of 5, 10, 20, 40, 80, 125 and 200 V s^{-1}. The simulated curves refer to the mechanism postulated in (R1)–(R3).

The reduction proceeds in a stepwise manner with two one-electron steps; the second step occurs at more positive potentials than the first and is so fast that only a lower limit can be estimated for k_s^0 in (R2).

$$\mathrm{Fe{-}Fe} + e \leftrightarrow {}^{-}\mathrm{Fe{-}Fe} \quad \left(U_1^0 = -1.505\ \mathrm{V};\ k_1^0 \approx 0.65\ \mathrm{cm/s}\right) \quad \text{(R1)}$$

$${}^{-}\mathrm{Fe{-}Fe} + e \leftrightarrow {}^{-}\mathrm{Fe{-}Fe}^{-} \quad \left(U_2^0 = -1.39\ \mathrm{V};\ k_2^0 > 1\ \mathrm{cm/s}\right) \quad \text{(R2)}$$

$${}^{-}\mathrm{Fe{-}Fe}^{-} \rightarrow Q \quad \left(k_{f3} \approx 1\ \mathrm{s}^{-1};\ k_{b3} \ll k_{f3}\right) \quad \text{(R3)}$$

The fact that the electron transfer results in a cleavage of the iron–iron bond is not considered in the above reaction scheme[21] because this information cannot unambiguously be extracted from the experimental CVs. There are only some indirect indications that a bond cleavage in (R1) could account for the higher energy and the slower rate constant associated with this reaction. It would also explain why the reoxidation of the reduced iron species does not proceed in a fully reversible manner. By convoluting the experimental CVs with $t^{-1/2}$ (a procedure called "semi-integration" in the electrochemical literature[21]) as shown in Figure S1[22] (see Supporting Information), it is revealed that the electrons consumed in the forward scan are almost completely regained in the backward scan, but about 3% of the iron species is reoxidised at a slightly more positive potential. This is an indication of the existence of an unknown decomposition product postulated in (R3). However, the effect was too small to examine the reoxidation process via the unknown product.

Electrochemistry of 3 in the Presence of Pivalic Acid

Figure 7 presents the CVs of **3** in acetonitrile (solid line) at different concentrations of pivalic acid. By looking at the semi-integrated curves shown in Figure S2[22], it is revealed that the overall number of electrons consumed in the forward scan up to about –1.55 V is independent of HP concentration. Consequently, the reduced iron species are not yet able to produce hydrogen from pivalic acid by homogeneous electron transfer in the potential range in which the

(heterogeneous) two-electron reduction proceeds. Moreover, the electrons consumed in the reduction process are completely regained in the backward scan irrespective of the HP concentration [except for a small difference that corresponds roughly to the amount assigned to the unknown product *Q* in reaction (R3)], but the overall reoxidation occurs in four processes (indicated by P2–P5 in Figure 7) if the acid is present.

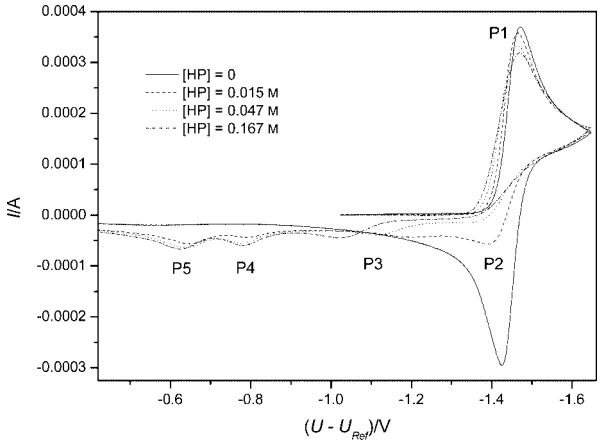

Figure 7. Cyclic voltammograms of 2.46 mM **3** in the absence and presence of pivalic acid. The scan rate is $v = 20\ V\,s^{-1}$.

Further reduction is observed when the potential scan is extended to negative potentials beyond –1.6 V, as can be seen in Figure 8a,b. The additional reduction process P6 at about –2.2 V is not observed in the absence of pivalic acid, and the current of this peak grows with increasing HP concentration. The most likely explanation for this observation is the catalytic reduction of pivalic acid to hydrogen, mediated by the iron complex. The importance of understanding the electrochemistry of the processes leading to the catalytic formation of hydrogen is revealed when **3** is considered as a model complex for the active site of [Fe-only]-hydrogenase.

Figure 7 makes it clear that the peaks associated with processes P2–P5 exhibit very different potential shifts as a function of the HP concentration. While P4 is rather independent of the HP concentration, a tenfold increase in [HP] results in a shift in P5 to more positive potentials by about 59/2 mV. The strongest dependence is observed for P3, where the potential shift is about three Nernst factors. The last observation could be explained by assuming that the charge-transfer reaction in P3 occurs in the form of a preceding chemical reaction caused by the dissociation of three HP molecules. Indeed, the current curve referring to [HP] = 0.015 M in Figure 7 shows the plateau shape expected for a preceding chemical reaction, but as the HP concentration increases, the curve becomes increasingly peak-shaped. It is therefore more likely that P3 represents a ladder scheme or that the equilibrium concentration of the species that is reoxidised is not negligibly small at higher HP concentrations.

In this paper we have mostly focussed on the reactions leading to P1, P2 and P3 in Figure 7 and to P6 in Figure 8. On looking at Figure 9, it can be seen that P1–P3 can be reproduced very well by adding the reactions to (R1)–(R2).

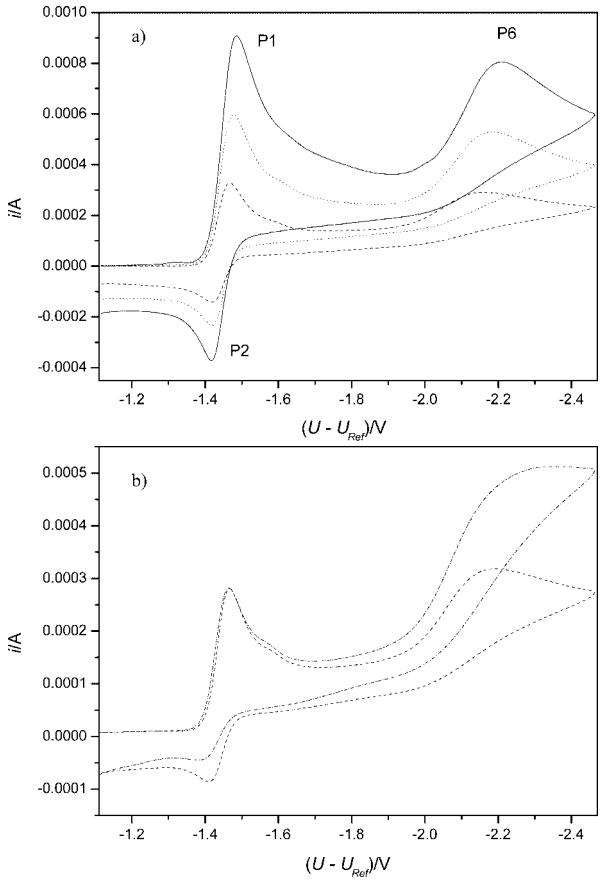

Figure 8. Cyclic voltammograms of **3** in the presence of pivalic acid. (a) 2.2 mM **3** and 10 mM HP, scan rate 20 $V\,s^{-1}$ (dashed line), 77 $V\,s^{-1}$ (dotted line) and 200 $V\,s^{-1}$ (solid line). (b) 2.0 mM **3** and 10 mM (dashed line) or 20 mM (dotted and dashed line) HP, scan rate 20 $V\,s^{-1}$.

It is important to emphasise that parameter couplings prevent the determination of some parameters in the above reaction scheme. This means that virtually the same standard deviation is obtained with different parameter combinations. Despite this uncertainty, the signature of the above reaction scheme is that it may serve as a basis for interpreting (at least qualitatively) the pathway leading to the catalytic generation of hydrogen shown in the CVs in Figure 8.

The reaction of the reduced iron species **3** in the presence of pivalic acid starts with the formation of 1:1 and 1:2 complexes. In the case of the monoanion, only the 1:1 complex needs to be considered because the equilibrium for reaction (R8) seems to lie far to the left. Actually, electrochemical methods such as cyclic voltammetry are not able to distinguish whether undissociated HP molecules are hydrogen-bonded in (R4)–(R7) and (R10) or if a proton transfer occurs as formulated here for (R4).

However, the fact that the ratio of the peak currents associated with P1 and P2 exhibits virtually no scan-rate dependence even when using only a relatively small excess of pivalic acid (see Figure 9a) can be explained only if the complex formation in (R4)–(R6) proceeds as an irreversible process where the effect of the dissociation reaction remains

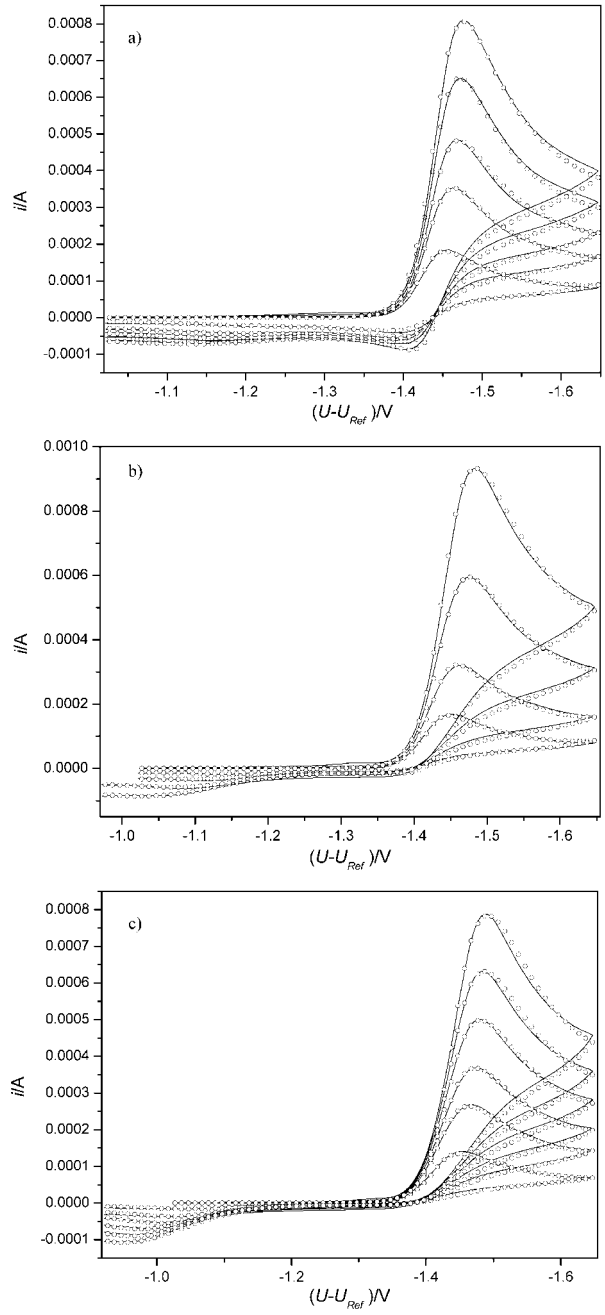

Figure 9. Experimental (solid lines) and simulated (open circles) CVs for the reduction of 2.46 mM **3** in the presence of pivalic acid. (a) [HP] = 0.015 mol L^{-1}; v = 5, 20, 40, 77, 125 V s^{-1}. (b) [HP] = 0.047 mol L^{-1}; v = 5, 20, 77, 200 V s^{-1}. (c) [HP] = 0.167 mol L^{-1}; v = 5, 20, 40, 77, 125, 200 V s^{-1}. The simulated curves refer to the mechanism postulated in (R4)–(R11), with n = 3 in (R7).

$$^{-}Fe-Fe + HP \rightarrow {}^{-}Fe-Fe(HP) \quad (K_4 >> 1; k_{f4} \approx 10^5\,M^{-1}s^{-1}) \quad (R4)$$

$$Fe-Fe + HP \rightarrow Fe-Fe(HP) \quad (K_5; k_{f5} \approx 10^5\,M^{-1}s^{-1}) \quad (R5)$$

$$^{-}Fe-Fe^{-}(HP) + HP \rightarrow {}^{-}Fe-Fe^{-}(HP)_2 \quad (K_5K_6 >> 1; k_{f6} >> k_{b5}) \quad (R6)$$

$$^{-}Fe-Fe^{-}(HP)_2 + nHP \leftrightarrow {}^{-}Fe-Fe^{-}(HP)_2[HP]_n \quad (K_7 \approx 55; k_{f7} \approx 3\times10^6\,M^{-1}s^{-1}) \quad (R7)$$

$$^{-}Fe-Fe(HP) + e \leftrightarrow {}^{-}Fe-Fe^{-}(HP) \quad (U_8^0 \approx -1.6\,V; k_8^0 \approx 0.3\,s^{-1}) \quad (R8)$$

$$^{-}Fe-Fe(HP)_2 + e \leftrightarrow {}^{-}Fe-Fe^{-}(HP)_2 \quad (U_9^0 \approx -1.09\,V; k_9^0 \approx 0.3\,s^{-1}) \quad (R9)$$

$$^{-}Fe-Fe(HP) + HP \leftarrow {}^{-}Fe-Fe(HP)_2 \quad (K_{10} << 1; k_{b10} >> 1) \quad (R10)$$

$$^{-}Fe-Fe^{-}(HP)_2[HP]_n \rightarrow Q^{*} \quad (k_{f11} \approx 4; k_{b11} << k_{f11}) \quad (R11)$$

$$^{-}Fe-Fe + HP \rightarrow Fe-Fe(H) + P^{-} \quad (R12)$$

negligibly small. The latter effect may rather be expected for the formation of a protonated species where the opposite charge of the ions counteracts the dissociation reaction. On the other hand, HP is a very weak acid in acetonitrile and is not dissociated. The pK_a value of acetic acid (which is rather a stronger acid) in anhydrous acetonitrile is only 22.3.[23] However, one should keep in mind that the basicity of the anions of **3** could be increased in the same way that the acidity of pivalic acid is decreased under anhydrous conditions. Nevertheless, it is unlikely that more protons are coordinated than that required to compensate for the negative charge of the reduced iron species, and it remains even questionable whether the dianion of **3** is a strong enough base for the deprotonation of two molecules of pivalic acid. For this reason, we prefer a neutral formulation Fe–Fe(HP), where (HP) in parenthesis represents either a strongly hydrogen-bonded HP molecule or a proton. This type of H^+/HP-bonding must be clearly distinguished from the weak and labile bonding of HP molecules postulated in (R7), for which square brackets are used.

Unfortunately, the number n of HP molecules coordinated in this step [R(7)] could not unambiguously be determined. The numbers reported in (R7) refer to n = 1. The problem is that the effect of reaction (R7) is mostly visible in P3, but the average height of the plateau current can be satisfactorily well reproduced with the values $1 \leq n \leq 3$. Thus, for instance, a standard deviation of s = 0.013 was obtained by fitting the experimental data based on reactions (R1), (R2) and (R4)–(R11) with n = 1, while a minimum of s = 0.012 was found for n = 3. This finding is not very significant. However, inspection of all simulated and experimental curves in the potential range associated with P3 reveals that the correct shift for the (half) peak potential of the plateau current as a function of HP concentration is attained only for n = 3, which is in agreement with the potential shift of about three Nernst factors mentioned above. It should be emphasised that we were not able to simulate the experimental data when only (R7) was used with n = 3 and (R5) and (R6) were omitted. We assumed a strong irreversible coordination in the first step and a weaker and labile coordination in the follow-up reaction.

The weak hydrogen bonding of three additional HP molecules could occur, for instance, at the sulfur centres of the molecule provided that the species postulated in (R7) is really a di- or at least a monoanion. Arguments supporting such an assumption can be found in the literature. For example, hydrogen bonding of three undissociated acid molecules at a radical monoanion was postulated in the reduction pathway of 3,5-di-*tert*-butyl-1,2-benzoquinone in the presence of 2,2,2-trifluoroethanol.[24]

Finally it should be mentioned that reaction (R11) plays a similar role to that of process P3 in the absence of pivalic acid. A somewhat larger rate constant was used for (R11), which is in agreement with the results from semi-integration shown in Figures S1 and S2[22].

We will now deal with the most critical question arising from the above reaction scheme: where do the additional processes P4 and P5 in Figure 7 come from? The most

straightforward explanation is that n in (R7) really equals 3 and that the three peaks represent the reoxidation processes associated with $n = 1$, 2 and 3 for the corresponding species not yet consumed in the dissociative pathway. Of course, this situation cannot be simulated on the basis of the above reaction scheme that takes only the gross reaction but not the successive complex formation steps into account. The description of more detailed investigations that focus particularly on these processes is beyond the scope of this paper. These findings will be published separately; a detailed knowledge of these processes does not seem to be necessary for the understanding of the pathway that leads to the catalytic current (P6) in Figure 8.

As a first step, this process was analysed by determining the number of electrons additionally consumed in the presence of pivalic acid in the potential range between –1.6 and –2.5 V. The latter was accomplished by semi-integrating the experimental CVs measured with a small excess of pivalic acid. Figure S3 (Supporting Information) shows the number of electrons, z, determined in this way as a function of the scan rate. It can be concluded that two additional electrons are consumed in this potential range in the limiting case $v \rightarrow \infty$, where the contributions of the catalytic reactions become negligibly small.

A more detailed analysis reveals that a catalytic process is still not detectable when only one more electron is transferred to the doubly reduced iron species (at least when working with a small excess of pivalic acid).

P6 is governed equally by heterogeneous and homogeneous charge-transfer reactions when as little as a fivefold excess and scan rates between 20 and 200 $V s^{-1}$ are used. Moreover, the formulation of feasible follow-up reactions is simplified by the fact that $^{-}$Fe–Fe^{-}(HP)$_2$ is the dominating species in the postulated reaction scheme. Hence, only two further reduction steps of this species were taken into consideration. On looking at Figure 8, it can be seen that the curve remains peak-shaped and no reoxidation process is visible in the potential range associated with P6, independent of the scan rate. Thus, at least the first reduction step (apparently not yet involved in a catalytic process) must be slow and fully irreversible. This could be explained by assuming that further reduction of the HP complexes proceeds as a concerted proton and electron transfer (CPET) reaction in which electron transfer from the electrode to the complex occurs simultaneously with proton transfer from a hydrogen-bonded HP molecule within the complex. CPET reactions have also been invoked for the electrochemical reduction of superoxide,[25] the oxidation of an amino phenol[26] and the oxidation of 1,4-hydrobenzoquinone-2,5-dicarboxylate.[27] Arguments supporting the CPET designation, rather than the possible two-step pathways, have been fully developed for each case.

Because of the perfect coupling between the heterogeneous rate constants and the standard potential for an irreversible charge-transfer process, the heterogeneous rate constants were set to more or less arbitrary values and the standard potential was then adjusted together with the charge-transfer coefficient to simulate the shape of the current curve, at least qualitatively. The following values were used: $U^0_{15} = -1.475$ V, $k^0_{15} = 10^{-3}$ cm s^{-1}, $\alpha_{15} \approx 0.25$; $U^0_{16} = -1.77$ V, $k^0_{16} = 1.2 \times 10^{-3}$ cm s^{-1}, $\alpha_{16} \approx 0.35$.

The assumption that the catalytic cycle is obtained by a reaction of type (R15), which forms a product that can then be directly re-reduced according to the pathway (R1), (R2), (R5), (R6), (R13) and (R14), is not in agreement with the experimental results.

$$^{-}Fe - Fe^{-}(HP)_2 + e \rightarrow {}^{-}H - Fe - Fe^{-}(HP) + P^{-} \quad (R13)$$

$$^{-}H - Fe - Fe^{-}(HP) + e \rightarrow {}^{-}H - Fe - Fe - H^{-} + P^{-} \quad (R14)$$

$$^{-}H - Fe - Fe - H^{-} + 2HP \rightarrow Fe - Fe + H_2 + 2P^{-} \quad (R15)$$

The assumption mentioned above inevitably leads to the situation in which the current curve does not remain peak-shaped for each scan rate. It becomes increasingly plateau-shaped, as expected for a first-order catalytic mechanism when the scan rate is reduced. Therefore, the shape of the peak for P6 in Figure 8 cannot result from a second-order catalytic reaction in which the depletion of HP accounts for the decay in the catalytic current after a maximum value is reached. A reasonable agreement between simulation and experiment could be obtained only by assuming that the species produced in the first catalytic step [R(16)] does not only undergo a catalytic regeneration reaction according to reactions R(17) or R(18), but also a deactivation reaction in the form of a slow irreversible charge-transfer step [R(19)] that results in the formation of a species that does not participate in the catalytic cycle. It is very possible that this species, simply denoted as $^{-}$H–Fe–Fe^{-}, is stabilised by hydrogen-bonded HP molecules or through follow-up reactions.

$$^{-}H - Fe - Fe - H^{-} + HP \xrightarrow{k_{f18}} {}^{-}H - Fe - Fe + H_2 + P^{-} \quad (R16)$$

$$^{-}H - Fe - Fe + HP \xrightarrow{k_{f19}} {}^{-}H - Fe - Fe(HP)$$

$$\xrightarrow{e} {}^{-}H - Fe - Fe^{-}(HP) \quad (R17)$$

$$^{-}H - Fe - Fe + 2HP \rightarrow {}^{-}Fe - Fe(HP)_2 + H \quad (R18)$$

$$^{-}H - Fe - Fe + e \rightarrow {}^{-}H - Fe - Fe^{-} \quad (R19)$$

This leads to the following situation: if the HP concentration is low, the current for the process P6 is governed by reactions (R16) and (R17), while the catalytic cycle [going from (R17) or (R18) back to (R13) or (R10), respectively] has a relatively small effect. The forward scan of the experimental CVs shown in Figure 8 can be reproduced very well for this limiting case by using $k_{f18} \approx 5 \times 10^6$ $M^{-1} s^{-1}$, $k_{f19} \leq 10^4$ $M^{-1} s^{-1}$ and the following charge transfer parameters for (R17) and (R19): $U^0 = -1.82$ V, $k^0 = 10^{-3}$ cm s^{-1}, $\alpha \approx 0.5$. However, because of the irreversibility of the reduction steps postulated in the catalytic cycle, the height of the curve for P2 is much smaller than that in the experimental CVs. Very good agreement for both scan segments can be attained if the product on the right-hand side of the last equation [R(19)] is reoxidised in two steps to **3**. As $^{-}$H–Fe–Fe^{-} is formally a triply reduced iron species, a follow-up

reaction (maybe with the release of hydrogen) has to occur before, after or in a concerted way with the charge transfer. The standard potential(s) and the heterogeneous rate constant(s) for the two reoxidation steps are not critical as long as this pathway remains much faster (in the potential range associated with P2) than the return of the species into the catalytic cycle by reactions (R13) and (R14). The CVs simulated for this limiting case (under the same experimental conditions as those for Figure 8a) are shown in Figure 10.

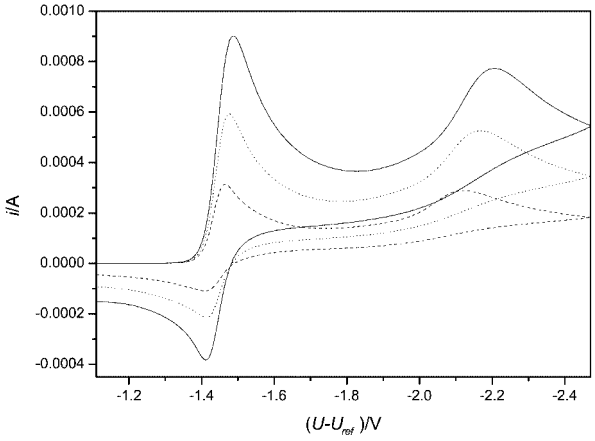

Figure 10. CVs simulated on the basis of (R13), (R14), (R17), (R18) and (R20) by using the same experimental conditions as those given for Figure 8 (a) and the kinetic parameters mentioned in the text.

By increasing the HP concentration, reactions (R17) or (R18) should be favoured, at the expense of reaction (R19). Consequently, the current for the process P6 should grow, while that for P2 becomes smaller. This exact result is observed in the experimental CVs shown in Figure 8 b. This effect and the fact that the height of the peak for P6 not only increases but also broadens when the HP concentration is doubled could be reproduced well in the simulated CVs shown in Figure 11.

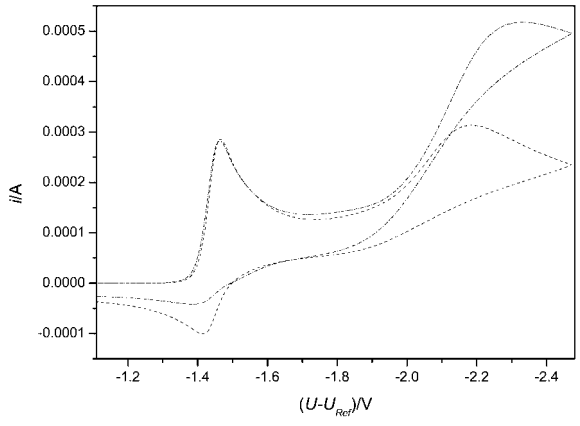

Figure 11. CVs simulated on the basis of (R13), (R14), (R17), (R18) and (R20) by using the same experimental conditions as those given for Figure 8b. Note, however, that different values for k_{f18} and k_{f19} were used in both curves to reproduce the most characteristic features of the experimental CVs.

However, the characteristic changes in the experimental CVs mentioned above could not be attained by repeating the simulations with twice the HP concentration with the same kinetic parameters as those for Figure 10. When the HP concentration is doubled, a simulated CV that matches the experimental CV was obtained with the parameters $k_{f18} \approx 10^5\ M^{-1}\,s^{-1}$ and $k_{f19} \approx 8 \times 10^6\ M^{-1}\,s^{-1}$ and by shifting the U^0_{15} value in a positive direction by about 0.1 V (a similar effect can also be achieved by analogously shifting the U^0_{21} value instead of varying k_{f19}).

In principle, this result is not surprising because only products derived from the 1:2 complex were considered to participate in the catalytic cycle. This means that the rate constants optimised in this way describe the overall effect of all HP complexes that can be activated in the catalytic cycle by reduction steps that are analogous to reactions (R13) and (R14). In the best case, such an approach applies to one particular HP concentration. Other more subtle effects may also play a role. For instance, the conditional standard potential for CPET reactions such as (R13) and (R14) is not independent of the HP concentration if the anions on both sides of the reaction are stabilised in different ways by hydrogen bonding to HP molecules. The results obtained on the basis of the simplified reaction scheme in this paper are therefore a promising first step worth pursuing in further studies.

Conclusions

The present study shows that the heterocyclic compounds **1**, **6**, **10** and **13** react with $Fe_2(CO)_9$ (**2**) by insertion along the S–S bond to provide novel model complexes for [Fe-only]-hydrogenase. The structures of the resulting products are dependent on the ring size of the heterocycles: the reaction with 1,2,4-trithiolane (**1**) yields the diiron complex **3** that adopts a structure quite similar to $Fe_2(PDT)(CO)_6$, $Fe_2(ADT)(CO)_6$ and $Fe_2(ODT)(CO)_6$.[6a–6g,6i,6l] The seven- and eight-membered heterocycles **6** and **13** lead to the three-iron clusters **7** and **13** with intramolecular coordination of the thioether moiety. Furthermore, we have demonstrated that the nine-membered ring compound **10** delivers a diiron complex containing the coordinating thioether. The structures can be attributed to the different flexibilities of the heterocycles **1**, **6**, **10** and **13**.

The electrochemical reduction of **3** proceeds through two reversible, one-electron steps. The second step is faster and has a more positive standard potential than the first. The chemical reversibility of these processes is lost after a weak Brønsted acid is added. In the case of pivalic acid, the experimental CVs can be explained by assuming that either two undissociated HP molecules are strongly coordinated to the dianion by hydrogen bonds or a neutral species is formed by proton transfer. Additionally, up to three HP molecules may be weakly coordinated by hydrogen bonds, but no catalytic hydrogen generation is observed in the potential range in which the two-electron reduction occurs.

Hydride species (usually considered as the catalytically active species in the literature) are generated in two further one-electron reduction steps. However, unlike most of the systems reported in the literature,[28] the hydrides of **3** are produced in slow and irreversible charge-transfer processes, which result in a well-separated current peak at a distinctly more negative potential. The latter may be attributed to the particularly low acidity of pivalic acid in acetonitrile under anhydrous conditions. The shape of this peak and the scan rate dependence of its height are not in agreement with the postulation of a catalytic cycle in which the direct regeneration of the electrocatalytically active species is the rate-determining step. The experimental curves could be reproduced sufficiently well by assuming that a deactivation reaction in the form of an irreversible charge-transfer reaction proceeds simultaneously with the regeneration of the electrocatalytically active species.

Experimental Section

General: The ^1H and $^{13}C\{^1H\}$ NMR spectra were recorded with a Bruker DRX 200 or DRX 400 spectrometer by using the solvent as a standard. 2D NMR spectra were recorded with the DRX 400 spectrometer. The mass spectra were recorded with a FINNIGAN MAT SSQ 710 instrument. The IR spectra (KBr pellet technique) were recorded with a Thermoelectron Nicolet AVATAR 30070 DTGS or with a Biorad FTF 25 apparatus (ATR cuvettes for neat samples). 1,2,4-Trithiolane (**1**),[29] 1,2,5-trithiepane (**6**), 1,2,6-trithionane (**10**) and 1,2,5-trithiocane (**13**)[14] were prepared according to literature protocols. Elemental analyses were performed with a LECO CHNS-932 apparatus. Solvents and $Fe_2(CO)_9$ (**2**) were purchased from Sigma–Aldrich. Tetrahydrofuran (thf) was dried with sodium/benzophenone before use. Reported yields refer to the amount of purified products. For column chromatography Merck Silica gel 60 (0.015–0.040 mm) was used. Merck TLC aluminium sheets silica gel 60 F_{254} were used for TLC.

$Fe_2(SDT)(CO)_6$ (3): Nonacarbonyldiiron (**2**) (2 g, 5.5 mmol) and 1,2,4-trithiolane (**1**) (227 mg, 1.83 mmol) were dissolved in thf (20 mL) and stirred at 65 °C for 15 min under argon. The colour of the light orange solution became deep red, and a brown solid (inorganic iron sulfides) precipitated. The reaction mixture was cooled to room temperature, and the solvent was removed under reduced pressure. The crude product was purified by column chromatography by using hexane as eluent. The orange fraction (R_f = 0.5) was collected, and the solvent was removed. The product was obtained as a red-orange solid. Crystals suitable for X-ray diffraction analysis were obtained by slow evaporation of a concentrated pentane solution of **3** into hexane at 0 °C. Product **3** was also crystallised from a solution of hexane at –25 °C. Yield 279 mg (37.8%). $C_8H_4Fe_2O_6S_3$ (404): calcd. C 23.78, H 0.99, S 23.81; found C 23.81, H 1.26, S 23.48. ^1H NMR (200 MHz, $CDCl_3$, 25 °C): δ = 3.21 (s, 4 H, CH_2) ppm. $^{13}C\{^1H\}$ NMR (100 MHz, $CDCl_3$): δ = 27.7 (*C*H_2), 206.79 (*C*O) ppm. FTIR (KBr): $\tilde{\nu}$ = 2075 (s), 2027 (s), 1999 (vs, νCO, terminal) cm^{-1}. MS (DEI = 70 eV): *m*/*z* (%) = 404 (16) [M^+], 376 (100) [M^+ – 28; CO], 348 (70) [M^+ – 56; 2 CO], 320 (46) [M^+ – 84; 3 CO], 292 (17) [M^+ – 112; 4 CO], 264 (42) [M^+ – 140; 5 CO], 236 (58) [M^+ – 168; 6 CO], 208 (58) [264 – 56; Fe], 176 (26) [208 – 32; S], 144 (68) [176 – 32; S], 122 (12) [144 – 32; S], 78 (8) [CH_2S_2], 56 (26), 45 (12) [CHS].

$Fe_3(BTES)(CO)_9$ (7): Nonacarbonyldiiron (**2**) (1.49 g, 4.08 mmol) and 1,2,5-trithiepane (**6**) (207 mg, 1.36 mmol) in thf (15 mL) were stirred at 65 °C for 15 min under argon. The colour of the light orange solution became deep green, and a brown solid (mixture of inorganic iron sulfides) precipitated. The reaction mixture was cooled to room temperature, and the solvent removed under reduced pressure. The crude brown product was purified by column chromatography with diethyl ether as eluent. The dark green fraction (R_f = 0.5) was collected, and the solvent removed. The product was obtained as a dark green solid. Crystals suitable for X-ray diffraction analysis were obtained by slow evaporation of a concentrated ether solution of **7** into hexane at 0 °C. Yield 327 mg (41.4%). $C_{13}H_8Fe_3O_9S_3$ (571.93): calcd. C 27.30, H 1.41, S 16.82; found C 27.26, H 1.65, S 16.65. ^1H NMR (400 MHz, $CDCl_3$, 25 °C): δ = 1.69 (ddd, $^2J_{AB}$ = 13.4, $^3J_{AC}$ = 19.6, $^3J_{AD}$ = 5.2 Hz, 2 H, $H_BH_ACSCH_AH_B$), 2.34 (ddd, $^2J_{CD}$ = 13.7, $^3J_{CA}$ = 19.6, $^3J_{CB}$ = 6.9 Hz, 2 H, SCH_CH_D), 3.13 (dd, $^2J_{AB}$ = 13.4, $^3J_{BC}$ = 6.9 Hz, 2 H, $H_BH_ACSCH_AH_B$), 3.27 (dd, $^2J_{CD}$ = 13.7, $^3J_{DA}$ = 5.2 Hz, 2 H, SCH_CH_D) ppm. $^{13}C\{^1H\}$ NMR (100 MHz, $CDCl_3$): δ = 39.7 (CH_2SCH_2), 45.6 (SCH_2CH_2), 202.5, 208.6, 211.1, 211.8, 213.7 (*C*O) ppm. FTIR (KBr): $\tilde{\nu}$ = 2073 (s), 2033 (vs), 1958 (vs, νCO, terminal) cm^{-1}. FTIR (ATR cuvette): $\tilde{\nu}$ = 2071 (s), 2034 (m), 2021 (m), 2001 (s), 1974 (s), 1968 (s), 1953 (s), 1939 (s, νCO, terminal) cm^{-1}. MS (DEI = 70 eV): *m*/*z* (%) = 572 (2) [M^+], 544 (1) [M^+ – 28; CO], 516 (3) [M^+ – 56; 2 CO], 488 (2) [M^+ – 84; 3 CO], 460 (2) [M^+ – 112; 4CO], 432 (2) [M^+ – 140; 5CO], 404 (5) [M^+ – 168; 6 CO], 376 (12) [M^+ – 196; 7 CO], 348 (12) [M^+ – 224; 8 CO], 316 (10) [M^+ – 252; 9 CO].

$Fe_2(BTPS)(CO)_5$ (11): Nonacarbonyldiiron (**2**) (1.01 g, 2.77 mmol) and 1,2,6-trithionane (**10**) (166 mg, 0.92 mmol) in thf (15 mL) were stirred for 15 min at 65 °C under argon. The colour of the light orange solution became red-brown, and a brown solid (inorganic iron sulfides) precipitated. The reaction mixture was cooled to room temperature, and the solvent removed under reduced pressure. The crude brown product was purified by column chromatography with diethyl ether as eluent. The red-brown fraction (R_f = 0.6) was collected, and the solvent removed. Product **11** was a brown solid, which was crystallised from a solution of hexane at –25 °C. Yield 56 mg (14.1%). $C_{11}H_{12}Fe_2O_5S_3$ (432.09): calcd. C 30.58, H 2.80, S 22.26; found C 31.03, H 3.15, S 22.02. ^1H NMR (400 MHz, $CDCl_3$, 25 °C): δ = 1.32 [m, 1 H, $H_BH_AC(6)SCH_AH_B$], 2.12 [ddd, ^2J = 15.5, ^3J = 10.1, ^3J = 4.5 Hz, 1 H, $H_BH_AC(6)SCH_AH_B$], 2.23 [t, ^2J = 11.8 Hz, 1 H, $CH_2C(5)H_CH_DCH_2$], 2.33–2.40 [m, 2 H, $CH_2C(5)H_CH_DCH_2$ and $SC(4)H_EH_F$], 2.44 [ddd, ^2J = 12.3, ^3J = 7.9, ^3J = 3.7 Hz, 2 H, $H_BH_AC(1)SCH_AH_B$], 2.76–2.87 [m, 3 H, $CH_2C(2)H_CH_DCH_2$ and $SC(3)H_EH_F$], 2.96 [ddd, ^2J = 11.8, ^3J = 7.4, ^3J = 3.7 Hz, 1 H, $SC(3)H_EH_F$], 3.19 [ddd, ^2J = 14.3, ^3J = 5.6, ^3J = 2.8 Hz, 1 H, $H_BH_AC(4)SCH_AH_B$] ppm. $^{13}C\{^1H\}$ NMR (100 MHz, $CDCl_3$): δ = 18.9 [*C*(5)], 27.0 [*C*(2)], 28.41, 28.47 [*C*(1), *C*(6)], 36.7 [*C*(3)], 37.6 [*C*(4)], 209.7, 211.9, 213.9 (*C*O) ppm. FTIR (ATR cuvette): $\tilde{\nu}$ = 2040 (s), 1952 (vs), 1906 (vs, νCO, terminal) cm^{-1}. MS (DEI = 70 eV): *m*/*z* (%) = 432 (10) [M^+], 404 (18) [M^+ – 28; CO], 376 (28) [M^+ – 56; 2 CO], 348 (46) [M^+ – 84; 3 CO], 320 (52) [M^+ – 112; 4 CO], 292 (97) [M^+ – 140; 5 CO].

$Fe_3(S(CH_2)_2S(CH_2)_3S)(CO)_8$ (13): Nonacarbonyldiiron (**2**) (1.315 g, 3.6 mmol) and 1,2,5-trithiocane (**12**) (200 mg, 1.2 mmol) in thf (20 mL) were stirred for 15 min at 65 °C under argon. The colour of the light orange solution became red-brown, and a brown solid (inorganic iron sulfides) precipitated. The reaction mixture was cooled to room temperature, and the solvent was removed under reduced pressure. The crude red-brown product was purified by column chromatography using diethyl ether as eluent. The main orange fraction (R_f = 0.9) was identified as complex **8** (yield:

154 mg, 34.5%), and the yield of the nonidentified green fractions was 57 mg. The red-brown fraction (R_f = 0.13) was collected, the solvent was removed and compound **13** was obtained as a red-brown solid. Crystals suitable for X-ray diffraction analysis were obtained by slow evaporation of pentane into a concentrated solution of **13** in chloroform at 0 °C. Yield 46 mg (6.8%). ^{1}H NMR (400 MHz, $CDCl_3$, 25 °C): δ = 1.64 [m, 1 H, $H_BH_AC(2)SCH_AH_B$], 2.48 [m, ^2J = 15.5, ^3J = 10.1, ^3J = 4.5 Hz, 1 H, $H_BH_AC(2)$-SCH_AH_B], 2.83–2.95 [m, 2 H, $CH_2C(4)H_CH_DCH_2$ and $H_BH_AC(3)$-SCH_AH_B], 3.10 [m, 1 H, $SC(5)H_EH_F$], 3.24 [m, 1 H, $H_BH_AC(4)$-SCH_AH_B], 3.44 [m, 1 H, $SC(5)H_EH_F$], 3.59 [m, 1 H, $SC(1)H_CH_D$], 3.68 [m, 1 H, $H_BH_AC(3)SCH_AH_B$], 3.88 [m, 1 H, $SC(1)H_CH_D$] ppm. $^{13}C\{^1H\}$ NMR (100 MHz, $CDCl_3$): δ = 25.4 [C(4)], 31.7 [C(3)], 34.5 [C(2)], 34.7 [C(3)], 36.9 [C(5)], 214.8 (*C*O) ppm. FTIR (ATR cuvette): $\tilde{\nu}$ = 2053 (s), 1982 (vs), 1962 (vs), 1938 (vs), 1920 (vs, νCO, terminal) cm^{-1}. MS (DEI = 70 eV): *m*/*z* (%) = 558 (2) [M$^+$], 530 (9) [M$^+$ – 28; CO], 502 (15) [M$^+$ – 56; 2 CO], 474 (5) [M$^+$ – 84; 3 CO], 446 (15) [M$^+$ – 112; 4 CO], 418 (48) [M$^+$ – 140; 5 CO].

Electrochemistry – Instrumentation and Procedures: Cyclic voltammetric measurements were conducted using a three-electrode technique with a home-built computer-controlled device based on a PCI 6110-E data acquisition board (National Instruments). The measurements were performed in acetonitrile (containing 0.25 M tetra-*n*-butylammonium perchlorate) under a blanket of solvent-saturated argon. The ohmic resistance, which had to be compensated for, was determined by measuring the impedance of the system at potentials where the faradaic current was negligibly small. Background correction was accomplished by subtracting the CVs of the blank electrolyte (containing the same concentration of supporting electrolyte) from the experimental CVs. The reference electrode was an Ag|AgCl electrode in acetonitrile containing 0.25 M tetra-*n*-butylammonium chloride. As recommended by IUPAC,[19] all data reported in this paper were referenced to the ferrocenium/ferrocene couple; the measurements were taken at the end of the experiments. The working electrode was a hanging mercury drop (*m* = 2.79 mg) produced by a CGME instrument (Bioanalytical Systems, Inc., West Lafayette, USA).

Theoretical CVs were simulated by using the DigiElch simulation package (www.DigiElch.de). The simulation algorithm used in this program has been described previously.[20]

Unless otherwise stated, all charge-transfer coefficients were assumed to be 0.5, and the diffusion coefficients of all iron species postulated in the reaction schemes were set to $(1.02 \pm 0.03) \times 10^{-5}$ cm^2 s^{-1}. This is the value determined for **3**. The diffusion coefficient of pivalic acid was estimated to be 2.5×10^{-5} cm^2 s^{-1}.

In a typical series of experiments, about 0.002 mol L^{-1} of the complex was employed for the measurements consisting of seven scan rates ranging from 5 to 200 V s^{-1} and six different HP concentrations ranging from 0.01 to 0.2 mol L^{-1}. All experimental curves were then used for finding a suitable mechanism by making use of DigiElch's nonlinear regression procedure. The standard deviation between simulated and experimental CVs was normalised with respect to the maximum peak current found in the experimental CV. Hence, an overall standard deviation of s = 0.01 means that the average difference between the simulated and experimental CVs is 1% of the (average) peak current.

Crystal Structure Determination: The intensity data for the compounds were collected with a Nonius KappaCCD diffractometer, using graphite-monochromated Mo-K_α radiation. Data were corrected for Lorentz and polarisation effects, but not for absorption effects.[30,31] The structures were solved by direct methods (SHELXS[32]) and refined by full-matrix least-squares techniques against F_o^2 (SHELXL-97[33]). For compound **10**, the hydrogen atoms were located by difference Fourier synthesis and refined isotropically. For other compounds, the hydrogen atoms were included at calculated positions with fixed thermal parameters. All non-hydrogen atoms were refined anisotropically.[32] The XP software (SIEMENS Analytical X-ray Instruments, Inc.) was used for structure representations.

Crystal Data for 3: $C_8H_4Fe_2O_6S_3$, M_r = 403.99 g mol^{-1}, red-brown prism, size 0.03 × 0.03 × 0.02 mm, monoclinic, space group $P2_1/m$, a = 6.8211(3), b = 13.3393(7), c = 7.8888(3) Å, β = 107.898(3)°, V = 683.05(5) Å^3, T = –90 °C, Z = 2, $\rho_{calcd.}$ = 1.964 g cm^{-3}, μ(Mo-K_α) = 25.96 cm^{-1}, F(000) = 400, 4305 reflections in h(–8/7), k(–17/16), l(–9/10), measured in the range 2.71° ≤ Θ ≤ 27.46°, completeness Θ_{max} = 99.8%, 1630 independent reflections, R_{int} = 0.033, 1389 reflections with $F_o > 4\sigma(F_o)$, 83 parameters, 0 restraints, $R1_{obs}$ = 0.025, wR_{2obs} = 0.060, $R1_{all}$ = 0.034, wR_{2all} = 0.063, GOF = 1.029, largest difference peak and hole: 0.352/–0.541 e Å^{-3}.

Crystal Data for 7: $C_{13}H_8Fe_3O_9S_3$, M_r = 571.92 g mol^{-1}, black prism, size 0.03 × 0.03 × 0.01 mm, orthorhombic, space group $P2_12_12_1$, a = 8.5561(3), b = 13.8497(7), c = 16.5594(6) Å, V = 1962.28(14) Å^3, T = –90 °C, Z = 4, $\rho_{calcd.}$ = 1.936 g cm^{-3}, μ(Mo-K_α) = 25.51 cm^{-1}, F(000) = 1136, 13746 reflections in h(–11/10), k(–16/17), l(–21/21), measured in the range 1.92° ≤ Θ ≤ 27.48°, completeness Θ_{max} = 99.8%, 4485 independent reflections, R_{int} = 0.123, 3575 reflections with $F_o > 4\sigma(F_o)$, 253 parameters, 0 restraints, $R1_{obs}$ = 0.063, wR_{2obs} = 0.150, $R1_{all}$ = 0.085, wR_{2all} = 0.164, GOF = 1.049, Flack-parameter –0.01(3), largest difference peak and hole: 1.417/–1.033 e Å^{-3}.

Crystal Data for 10: $C_6H_{10}S_3$, M_r = 178.32 g mol^{-1}, colourless prism, size 0.10 × 0.10 × 0.06 mm, monoclinic, space group $P2_1/c$, a = 9.4696(6), b = 12.4325(9), c = 7.8849(3) Å, β = 113.932(3)°, V = 848.49(9) Å^3, T = –90 °C, Z = 4, $\rho_{calcd.}$ = 1.396 g cm^{-3}, μ(Mo-K_α) = 7.88 cm^{-1}, F(000) = 376, 5708 reflections in h(–12/11), k(–14/16), l(–9/10), measured in the range 2.35° ≤ Θ ≤ 27.49°, completeness Θ_{max} = 99.1%, 1937 independent reflections, R_{int} = 0.045, 1346 reflections with $F_o > 4\sigma(F_o)$, 91 parameters, 0 restraints, $R1_{obs}$ = 0.041, wR_{2obs} = 0.097, $R1_{all}$ = 0.072, wR_{2all} = 0.112, GOF = 1.040, largest difference peak and hole: 0.272/–0.374 e Å^{-3}.

Crystal Data for 11: $C_{11}H_{12}Fe_2O_5S_3$, M_r = 432.09 g mol^{-1}, red-brown prism, size 0.06 × 0.06 × 0.05 mm, monoclinic, space group $P2_1/c$, a = 10.2933(5), b = 9.3713(4), c = 16.2889(6) Å, β = 90.898(3)°, V = 1571.06(12) Å^3, T = –90 °C, Z = 4, $\rho_{calcd.}$ = 1.827 g cm^{-3}, μ(Mo-K_α) = 22.59 cm^{-1}, F(000) = 872, 10241 reflections in h(–13/12), k(–12/10), l(–20/20), measured in the range 1.98° ≤ Θ ≤ 27.48°, completeness Θ_{max} = 99.2%, 3567 independent reflections, R_{int} = 0.047, 2681 reflections with $F_o > 4\sigma(F_o)$, 190 parameters, 0 restraints, $R1_{obs}$ = 0.033, wR_{2obs} = 0.069, $R1_{all}$ = 0.0560, wR_{2all} = 0.078, GOF = 0.967, largest difference peak and hole: 0.361/–0.445 e Å^{-3}.

Crystal Data for 13: $C_{13}H_{10}Fe_3O_8S_3$, M_r = 557.94 g mol^{-1}, red-brown prism, size 0.05 × 0.05 × 0.05 mm, monoclinic, space group $P2_1/c$, a = 13.8117(6), b = 9.5857(4), c = 14.9198(7) Å, β = 100.243(4)°, V = 1943.82(15) Å^3, T = –90 °C, Z = 4, $\rho_{calcd.}$ = 1.907 g cm^{-3}, μ(Mo-K_α) = 25.68 cm^{-1}, F(000) = 1112, 12736 reflections in h(–16/17), k(–11/12), l(–19/17), measured in the range 3.07° ≤ Θ ≤ 27.49°, completeness Θ_{max} = 99.1%, 4422 independent reflections, R_{int} = 0.052, 3214 reflections with $F_o > 4\sigma(F_o)$, 244 parameters, 0 restraints, $R1_{obs}$ = 0.046, wR_{2obs} = 0.101, $R1_{all}$ = 0.076, wR_{2all} = 0.112, GOF = 1.021, largest difference peak and hole: 1.084/–0.638 e Å^{-3}.

CCDC-630342 (for **3**), -630343 (for **7**), -630344 (for **10**), -631279 (for **11**) and -631280 (for **13**) contain the supplementary crystallographic data for this paper. These data can be obtained free of charge from The Cambridge Crystallographic Data Centre via www.ccdc.cam.ac.uk/data_request/cif.

Supporting Information (see footnote on the first page of this article)(see also the footnote on the first page of this article): Two figures with semi-integral curves of experimental cyclic voltammograms[22] and a figure showing the overall number of electrons consumed at –2.5 V.

Acknowledgments

Financial support for this work was provided by the Freistaat Thüringen (Landesgraduiertenstipendium to J. W.). We are grateful to Prof. K. Ruhlandt-Senge for valuable discussions.

[1] G. Mloston, J. Romanski, H. P. Reisenauer, G. Maier, *Angew. Chem.* **2001**, *113*, 401–404; *Angew. Chem. Int. Ed.* **2001**, *40*, 393–396.

[2] a) A. Ishii, T. Akazawa, M.-X. Ding, T. Honjo, J. Nakayama, M. Hoshino, M. Shiro, *J. Am. Chem. Soc.* **1993**, *115*, 4914–4915; b) A. Ishii, T. Akazawa, T. Maruta, J. Nakayama, M. Hoshino, M. Shiro, *Angew. Chem. Int. Ed. Engl.* **1994**, *33*, 777–779.

[3] W. Weigand, S. Bräutigam, G. Mloston, *Coord. Chem. Rev.* **2003**, *245*, 167–175 and ref. cited therein.

[4] a) S. M. Aucott, H. L. Milton, S. D. Robertson, A. M. Z. Slawin, G. B. Walker, J. D. Woollins, *Chem. Eur. J.* **2004**, *10*, 1666–1676; b) S. M. Aucott, P. Kilian, S. D. Robertson, A. M. Z. Slawin, J. D. Woollins, *Chem. Eur. J.* **2006**, *12*, 895–902; c) S. M. Aucott, P. Kilian, H. L. Milton, S. D. Robertson, A. M. Z. Slawin, J. D. Woollins, *Inorg. Chem.* **2005**, *44*, 2710–2718; d) A. Ishii, M. Saito, M. Murata, J. Nakayama, *Eur. J. Org. Chem.* **2002**, 979–982; e) A. Ishii, T. Kawai, M. Noji, J. Nakayama, *Tetrahedron* **2005**, *61*, 6693–6699; f) A. Ishii, M. Murata, H. Oshida, K. Matsumoto, J. Nakayama, *Eur. J. Inorg. Chem.* **2003**, 3716–3721.

[5] a) Y. Nicolet, A. L. de Lacey, X. Vernède, V. M. Fernandez, E. C. Hatchikian, J. C. Fontecilla-Camps, *J. Am. Chem. Soc.* **2001**, *123*, 1596–1601; b) Y. Nicolet, B. J. Lemon, J. C. Fontecilla-Camps, J. W. Peters, *Trends Biochem. Sci.* **2000**, *25*, 138–143; c) Y. Nicolet, C. Piras, P. Legrand, C. E. Hatchikian, J. C. Fontecilla-Camps, *Structure* **1999**, *7*, 13–23.

[6] a) X. Zhao, I. P. Georgakaki, M. L. Miller, J. C. Yarbrough, M. Y. Darensbourg, *J. Am. Chem. Soc.* **2001**, *123*, 9710–9711; b) F. Gloaguen, J. D. Lawrence, M. Schmidt, S. R. Wilson, T. B. Rauchfuss, *J. Am. Chem. Soc.* **2001**, *123*, 12518–12527; c) E. J. Lyon, I. P. Georgakaki, J. H. Reibenspies, M. Y. Darensbourg, *J. Am. Chem. Soc.* **2001**, *123*, 3268–3278; d) M. Razavet, S. C. Davies, D. L. Hughes, J. E. Barclay, D. J. Evans, S. A. Fairhurst, X. Liu, C. J. Pickett, *Dalton Trans.* **2003**, 586–595; e) J. D. Lawrence, H. Li, T. B. Rauchfuss, M. Benard, M.-M. Rohmer, *Angew. Chem. Int. Ed.* **2001**, *40*, 1768–1771; f) H. Li, T. B. Rauchfuss, *J. Am. Chem. Soc.* **2002**, *124*, 726–727; g) S. Ott, M. Kritikos, B. Åkermark, L. Sun, *Angew. Chem. Int. Ed.* **2003**, *42*, 3285–3288; h) C. Tard, X. Liu, S. K. Ibrahim, M. Bruschi, L. De Gioia, S. C. Davies, X. Yang, L.-S. Wang, G. Sawers, C. J. Pickett, *Nature* **2005**, *433*, 610–613; i) L.-C. Song, Z.-Y. Yang, H.-Z. Bian, Q.-M. Hu, *Organometallics* **2004**, *23*, 3082–3084; j) D. Seyferth, R. S. Henderson, L.-C. Song, *Organometallics* **1982**, *1*, 125–133; k) D. Seyferth, R. S. Henderson, L.-C. Song, *J. Organomet. Chem.* **1980**, *192*, C1; l) L.-C. Song, Z.-Y. Yang, H.-Z. Bian, Y. Liu, H.-T. Wang, X.-F. Liu, Q.-M. Hu, *Organometallics* **2005**, *24*, 6126–6135; m) M. Y. Darensbourg, E. J. Lyon, J. J. Smee, *Coord. Chem. Rev.* **2000**, *206–207*, 533–561; n) R. C. Linck, T. B. Rauchfuss in *Bioorganometallics* (Ed.: D. Jaouen), Wiley-VCH, Weinheim, **2006**, 403–435; o) X. Zhang, C. Y. Chiang, M. L. Miller, M. V. Rampersad, M. Y. Darensbourg, *J. Am. Chem. Soc.* **2003**, *125*, 518–524; p) J. D. Lawrence, H. Li, T. B. Rauchfuss, *Chem. Commun.* **2001**, 1482–1483; q) L. C. Song, J. Gao, H. T. Wang, Y. J. Hua, H. T. Fan, X. G. Zhang, Q. M. Hu, *Organometallics* **2006**, *25*, 5724–5729.

[7] J. W. Tye, M. Y. Darensbourg, M. B. Hall, *Inorg. Chem.* **2006**, *45*, 1552–1559.

[8] A. Shaver, P. J. Fitzpatrick, K. Steliou, J. S. Butler, *J. Am. Chem. Soc.* **1979**, *101*, 1313–1315.

[9] R. Seidel, B. Schnautz, G. Henkel, *Angew. Chem. Int. Ed. Engl.* **1996**, *35*, 1710–1712.

[10] a) J. Messelhäuser, K. U. Gutensohn, I.-P. Lorenz, W. Hiller, *J. Organomet. Chem.* **1987**, *321*, 377–388; b) J. Messelhäuser, K. Haug, I.-P. Lorenz, W. Hiller, *Z. Naturforsch., B: Chem. Sci.* **1985**, *40*, 1064.

[11] S. Rossi, K. Kallinen, J. Pursiainen, T. T. Pakkanen, T. A. Pakkanen, *J. Organomet. Chem.* **1992**, *440*, 367–387.

[12] R. D. Adams, J. H. Yamamoto, *Organometallics* **1995**, *14*, 3704–3711.

[13] W.-F. Liaw, C.-Y. Chiang, G.-H. Lee, S. M. Peng, C.-H. Lai, M. Y. Darensbourg, *Inorg. Chem.* **2000**, *39*, 480–484.

[14] M. H. Goodrow, W. K. Musker, *Synthesis* **1981**, 457–459.

[15] A. F. Holleman, N. Wiberg, *Lehrbuch der Anorganischen Chemie*, Walter de Gruyter Verlag, Berlin, **1995**.

[16] M. Razavet, S. C. Davies, D. L. Hughes, C. J. Pickett, *Chem. Commun.* **2001**, 847–848.

[17] S. J. Borg, Th. Behrsing, S. P. Best, M. Razavet, X. Liu, C. J. Pickett, *J. Am. Chem. Soc.* **2004**, *126*, 16988–16999.

[18] a) F. Gloaguen, J. D. Lawrence, T. B. Rauchfuss, *J. Am. Chem. Soc.* **2001**, *123*, 9476–9477; b) F. Gloaguen, J. D. Lawrence, T. B. Rauchfuss, M. Bénard, M.-M. Rohmer, *Inorg. Chem.* **2002**, *41*, 6573–6582; c) D. Chong, I. P. Georgakaki, R. Meía-Rodríguez, J. Sanabria-Chinchilla, M. P. Soriaga, M. Y. Darensbourg, *Dalton Trans.* **2003**, 4158–4163.

[19] G. Gritzner, J. Kuta, *Pure Appl. Chem.* **1982**, *54*, 1527–1532.

[20] M. Rudolph, *J. Comput. Chem.* **2005**, *26*, 1193–1204, and literature cited therein.

[21] C. Greco, G. Zampella, L. Bertini, M. Bruschi, P. Fantucci, L. de Gioia, *Inorg. Chem.* **2007**, *46*, 108–116.

[22] A. J. Bard, L. R. Faulkner, *Electrochemical Methods, Fundamentals and Applications*, 2nd ed., John Wiley & Sons, New York, **2001**, pp. 247–252.

[23] G. A. N. Felton, R. S. Glass, D. L. Lichtenberger, D. H. Evans, *Inorg. Chem.* **2006**, *45*, 9181–9184.

[24] N. A. Macìas-Ruvalcaba, N. Okumura, D. H. Evans, *J. Phys. Chem. B* **2006**, *110*, 22043–22047.

[25] a) C. Costentin, D. H. Evans, M. Robert, J.-M. Savéant, P. S. Singh, *J. Am. Chem. Soc.* **2005**, *127*, 12490–12491; b) P. S. Singh, D. H. Evans, *J. Phys. Chem. B* **2006**, *110*, 637–644.

[26] C. Costentin, M. Robert, J.-M. Savéant, *J. Am. Chem. Soc.* **2006**, *128*, 4552–4553.

[27] C. Costentin, M. Robert, J.-M. Savéant, *J. Am. Chem. Soc.* **2006**, *128*, 8726–8727.

[28] a) J. F. Capon, F. Gloaguen, Ph. Schollhammer, J. Talarmin, *Coord. Chem. Rev.* **2005**, *249*, 1664–1676 and literature cited therein; b) X. Liu, S. K. Ibrahim, C. Tard, C. J. Pickett, *Coord. Chem. Rev.* **2005**, *249*, 1641–1652; c) D. J. Evans, C. J. Pickett, *Chem. Soc. Rev.* **2003**, *32*, 268–275.

[29] F. Asinger, M. Thiel, G. Lipfert, *Justus Liebigs Ann. Chem.* **1959**, *627*, 195.

[30] *COLLECT*, Data Collection Software, Nonius B. V., Netherlands, **1998**.

[31] Z. Otwinowski, W. Minor, "Processing of X-ray Diffraction Data Collected in Oscillation Mode" in *Methods in Enzymology*, Vol. 276, *Macromolecular Crystallography*, Part A

(Eds. C. W. Carter, R. M. Sweet), Academic Press, New York, **1997**, pp. 307–326.
[32] G. M. Sheldrick, *Acta Crystallogr., Sect. A: Found. Crystallogr.* **1990**, *46*, 467–473.
[33] G. M. Sheldrick, *SHELXL-97 (Release 97–2)*, University of Göttingen, Germany, **1997**.

Received: January 15, 2007
Published Online: April 24, 2007

